Power Electronic Drives for Magnetically Triggered Gels

Deron K. Jackson, Steven B. Leeb, *Member, IEEE*, Ahmed H. Mitwalli, Paolo Narvaez, Dahlene Fusco, and Elmer C. Lupton, Jr.

***Abstract*—Properly fabricated polymer gels exhibit an abrupt change in volume in response to a small change in an environmental parameter, such as temperature. We have developed gels that change in volume in response to an applied alternating magnetic field, and we are working to apply these gels as actuators. This paper describes power electronic circuits suitable for electromagnetic activation of these polymer gels. Issues in the selection of circuit topologies for this application are discussed. Experimental results are presented, which demonstrate magnetic activation of gels using prototype power electronic drives.**

***Index Terms*—Gel polymers, induction heating.**

I. Introduction

GELS CONSIST of a crosslinked network of polymers suspended in a solvent [1]. Under certain conditions, gels have been observed to undergo reversible changes in volume. These volume changes may be over 1000-fold and can be triggered by a variety of electrochemical conditions, including changes in temperature, solvent composition, or pH [2]–[4]. Gels could, in principle, be used as actuators in servomechanisms and sensors, which range in size from microscopic (silicon) mechanisms to mechanisms comparable in size and force density to biological systems. For example, polymer gels could act as synthetic muscles that provide direct, quiet, and swift linear motion with useful force densities [5]. Gels loaded with appropriate, beneficial solvents could be used in controlled drug-release applications either *in vivo* or *in vitro*. The many potential applications for gels are due, in part, to the wide range of environmental triggers for which gels can be made to respond.

This paper describes new techniques for remotely triggering gels using magnetic fields. Demonstration systems have been developed for each technique and will be described below. Power electronic drives were chosen and implemented to create an alternating magnetic field which heats a ferromagnetic "seed" material embedded in a gel. The magnetic field raises the temperature of the ferromagnetic material through a combination of loss mechanisms. The heated material, in turn, raises the temperature of the surrounding gel and triggers a volume phase transition. When the field is removed, the seed/gel system cools, and the volume phase transition reverses. Because the energy transfer to the seed/gel system occurs through a magnetic field, the system is contactless. It could be used to trigger a gel under the skin or in any remote location where an electromagnetic field could penetrate.

A quasi-static magnetic field is used to excite losses in the seed material. Quasistatic implies that the excitation field frequency (ranging from 240 kHz to 3 MHz in the prototypes) is small compared to the speed of light divided by the largest length D in the system. This is equivalent to saying that the primary energy storage and transfer occurs through the magnetic field [6]. We note, however, that it is possible to achieve similar triggering of a gel with a time-varying, quasistatic electric field (e.g., through dielectric losses in a carefully chosen seed material) or with a radiating electromagnetic wave. This paper focuses on magnetic field systems.

II. Gel Design

Experimentation was conducted with gels composed of N-isopropylacrylamide (NIPA). Gels were prepared by a free radical polymerization process in water with NIPA monomer, a crosslinker, and an appropriate polymerization initiator and accelerator. Typical formulas for the preparation of this widely studied gel are presented in [4]. Pre-gel solutions were permitted to polymerize in capillary tubes of 1.073 mm in diameter. After gelation, the gels are removed from the capillary tubes and washed to remove residual chemicals. The gels are then placed in a solvent, typically deionized water, for experimentation.

If an appropriate seed material is incorporated in or around the gel matrix, at least three loss mechanisms will induce heating from a magnetic field. The loss mechanisms include ohmic heating from eddy currents, hysteresis losses, and mechanical (frictional) losses. Depending on the approach, this seed material could be incorporated during or after gel formation. Three seeding methods will be considered below.

A. Method 1—Lumped Seed Material

The gel is seeded, for example, by inserting a short segment of a conductive, possibly ferromagnetic, material directly into the gel sample. Due to the macroscopic size of the

Manuscript received April 15, 1996; revised August 13, 1996. This work was supported in part by the MRSEC Program of the National Science Foundation under Award Number DMR-9 400 334, by the Massachusetts Institute of Technology Carl Richard Soderberg Career Development Chair, and by a New Venture Grant from AT&T Corporation. Test equipment for this work was made available through grants from the Intel Corporation and Tektronix.

D. K. Jackson, S. B. Leeb, A. H. Mitwalli, P. Narvaez, and D. Fusco are with the Laboratory for Electromagnetic and Electronic Systems, Massachusetts Institute of Technology, Cambridge, MA 02139 USA.

E. C. Lupton, Jr. is with Gel Sciences Corporation, Bedford, MA 01730 USA.

Publisher Item Identifier S 0278-0046(97)02825-6.

seed, significant heating can be induced with moderate field strength at frequencies of only a few hundred kilohertz. Ohmic heating from eddy currents tends to be the dominant loss mechanism with this approach. Induced losses are strongly dependent on the shape, conductivity, and permeability of the seed target. An excellent analysis of the relative heating efficiencies of ferromagnetic, cylindrically shaped seeds with varying material properties and form factors is presented in [7].

B. Method 2—Distributed or Powdered Seed Material

In this approach, the gel is seeded with conductive powder or flakes which are small compared to the gel dimensions. In our experiments, a concentration of ferromagnetic particles, approximately 5% by weight (0.5% by volume), is first coated with polyvinyl alcohol (PVA) and then mixed into the pre-gel solution. We have found that coating with PVA or a similar polymer is essential to ensure good suspension and dispersal of the metal flakes during the free radical polymerization process [8]. When the gel is formed, these particles are permanently trapped in the crosslinked polymer network. Particle shape and material properties must be selected carefully to provide desired heating, which comes primarily from eddy current and hysteresis losses. Our experiments with readily available commercial powders have revealed that ferromagnetic nickel flakes (approximately 30 μm in diameter and 0.4 μm in thickness) sold by Novamet[1] provided maximal heating at the given concentration and magnetic excitation described in the next sections. These observations agree qualitatively with published results in [9].

C. Method 3—Ferrofluid Solvent

In methods 1 and 2, the seed material is entrained in the polymer matrix. During a phase transition, the polymer network collapses around the seed material(s) as the gel solvent, deionized water, leaves the interstitial spaces of the polymer network. In method 3, the gel is not seeded by a trapped material as in methods 1 and 2. Instead, the solvent is replaced by a ferrofluid. A typical ferrofluid is composed of water, a surfactant, and a small amount (1%–4% by volume) of microscopic ferromagnetic material (roughly 87 Å across). The surfactant suspends the ferromagnetic particulants and prevents them from separating out of the mixture. When used as a gel solvent, ferrofluid diffuses into the expanded gel. The microscopic ferromagnetic particles fill and surround the expanded polymer network. We have found that when ferrofluid is excited by a strong magnetic field in the 2–3-MHz range, significant heating occurs. Microscopic mechanical motion may be a substantial source of dissipation in this method.

III. Experimental Overview

The diagrams in Fig. 1 outline the basic test stand used for all experiments. It may be helpful to refer to these diagrams throughout the discussion in this section. An ac inverter is used to generate a high-frequency voltage waveform from a dc voltage source. The voltage waveform is impressed across the terminals of a solenoid (see Fig. 1). The applied ac voltage causes an alternating current to flow in the winding, which in turn generates a high-frequency alternating magnetic field inside the coil. For a finite length solenoid, the time-varying magnetic field $H(t)$ at the center of the coil is

$$H(t) = \left[\frac{l/d}{\sqrt{1+(l/d)^2}}\right]\frac{Ni(t)}{l} \tag{1}$$

where N is the number of turns in the coil, $i(t)$ is the coil current, and l and d are the length and diameter of the coil, respectively. Note that in a practical field application, other magnetic coil arrangements, e.g., a Helmholtz coil pair, could be employed instead of the solenoid. High-frequency high-permeability materials could be used with a winding, or winding set, to guide magnetic flux to a target location.

The solenoid in our experiments is formed of litz wire wound on a triple-walled test vessel. As Fig. 1 illustrates, temperature-controlled cooling water circulates in the outer jacket of the test vessel to prevent coil heat from influencing the temperature of the inner test chamber. An insulating air space separates the inner test chamber from the outer water jacket. Finally, a sample under test, such as a gel and its solvent, is inserted into the test chamber. The magnetic field created by the solenoid is used in our experiments to excite

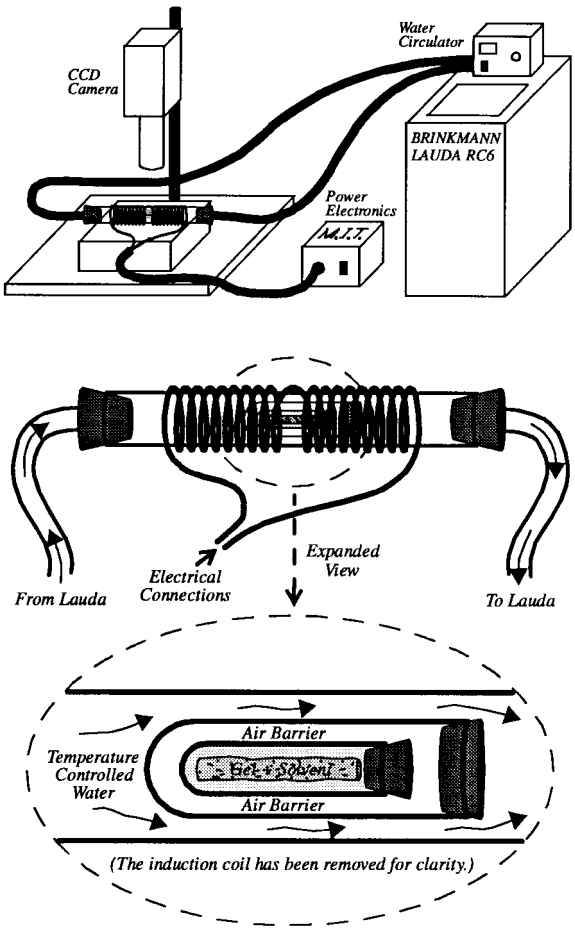

Fig. 1. The experimental setup with a close-up of the solenoid/gel assembly.

[1]Novamet Specialty Products Corporation, 10 Lawlins Park, Wyckoff, NJ 07481 USA.

losses in the target seed material in the test chamber. Three predominant loss mechanisms are considered below (see [6], [10], and [11] for more details).

A. Eddy Currents

High-frequency magnetic fields induce eddy currents in conductive materials. At sufficiently high frequencies, these currents flow in a thin surface region because of skin effect and can result in substantial ohmic power dissipation. When this surface region is small compared to the dimensions of the target seed, the current can be modeled with reasonable accuracy as flowing uniformly in a region with a depth equal to the "skin depth." The externally applied magnetic field is essentially excluded from the interior, bulk regions of the seed, i.e., from regions located several skin depths from the surface. The skin depth for a magnetically linear material is

$$\delta = \sqrt{\frac{2}{\omega\mu\sigma}} \tag{2}$$

where ω is the magnetic excitation frequency, μ is the magnetic permeability of the material, and σ is the conductivity of the material.

During early experimentation with different power electronic drives and coil configurations, single cylinders of test materials were employed in the test stand to verify theoretical heating predictions and circuit performance. These tests were functionally identical to the heating techniques outlined above in method 1. Consider, for example, an enamel-coated, type–4403 aluminum rod (25.4 mm in length and 1.59 mm in diameter) in 2 cc of deionized water in the induction heating test stand. Gels used in our experiments were often well over 90% water by volume, so the performance of a cylinder of seed material in pure water is a reasonable indicator of anticipated performance in a gel. (Due to an increase in skin depth and, thus, reduced ohmic losses, a nonferromagnetic seed like aluminum generally provides inferior heating when compared to an otherwise similar but ferromagnetic seed. However, aluminum is magnetically linear, and empirically observed heating performance can, therefore, be reconciled with analytical predictions.)

In the experiments with the aluminum rod, a 2.46-MHz sinusoidal magnetic field with a peak strength of 3900 A · T/m was applied axially by the solenoid in the test stand. Type-4403 aluminum has a measured conductivity of 2.87×10^7 mho/m and, at this frequency, exhibits a skin depth of approximately 60 μm. The ohmic power dissipation can be computed by solving precisely for the field and current distributions in the rod and then integrating a continuum version of Ohm's Law in the current-carrying regions. This approach is taken, for example, in the analyzes presented in [11] and [12]. Since the skin depth is relatively small, we employ a simplification that gives excellent results in comparison to the exact solution (in terms of Bessel's functions) of the magnetic diffusion equation in cylindrical coordinates.

We assume that the external, axial magnetic H-field is terminated by a uniform current density J flowing in the skin region and that the current density and H-field in deeper, interior regions of the rod are zero. The magnitude of the current density can be approximated by first finding an azimuthal surface current of magnitude K sufficient to terminate the externally applied H-field and then distributing this surface current uniformly over the width of a skin depth. Applying the appropriate magnetic field boundary condition at the surface of the rod, we find that $K = H_o$, where H_o is the magnitude of the external axial H-field. The current density J is approximately K/δ, and the instantaneous ohmic dissipation $P(t)$ can now be found by applying a continuum version of Ohm's Law integrated over the thin shell of volume V in which current flows, as follows:

$$P(t) = \frac{J^2}{\sigma}V = \frac{K^2}{\sigma\delta^2}V. \tag{3}$$

Under the assumption that the current flows entirely in a region the thickness of one skin depth, the volume of the thin shell is

$$V = \pi(r^2 - (r-\delta)^2)h \tag{4}$$

where r and h are the radius and length of the rod, respectively. The H-field applied in our experiments varies sinusoidally with time. The steady-state time-averaged power dissipation P_{diss} may, therefore, be found by replacing the peak surface current K with the rms surface current $K_{\text{rms}} = K/\sqrt{2}$ as follows:

$$P_{\text{diss}} = \frac{K_{\text{rms}}^2}{\sigma\delta^2}V. \tag{5}$$

For the type-4403 sample described above, with a peak induction coil current of 8.88 A and externally applied peak H-field of 3900 A · T/m, the final temperature in the 2-cc water bath was 10.87 °C above ambient. Using (5), we compute a predicted steady-state power dissipation in the rod of $P_{\text{diss}} =$ 0.539 W.

To verify the accuracy of the computed power dissipation, we replaced the rod in the 2-cc water vessel with an ohmic resistor driven from a dc supply. With the induction coil deactivated, a power dissipation of 0.555 W in the resistor was required to achieve the same 10.87 °C temperature rise as in the induction heating experiment. We presume that this power dissipation level is the actual power dissipated in the aluminum rod during our induction heating experiments. The predicted power dissipation is within 2.9% of this actual dissipation.

Several factors complicate the calculation of eddy current power dissipation when the seed material is not a single, relatively long rod. Closed-form determination of the externally applied field may be difficult when the seed material is irregularly shaped. Also, neighboring seeds can locally distort the magnetic field around a particular seed, complicating the determination of the externally applied H-field. If the seed material is ferromagnetic with a nonlinear magnetization characteristic, the classic linear solution of the magnetic diffusion equation employing skin depth is inaccurate. Approaches for dealing with nonlinear magnetization typically follow the approach introduced in [13], involving substantial simplification of the material behavior.

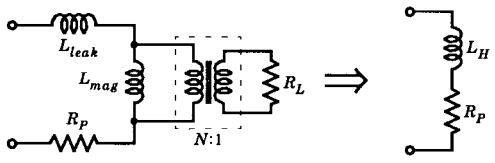

Fig. 2. Simplified load model.

B. Hysteresis Losses

An applied time-varying magnetic field constantly reorients the domains in a ferromagnetic material. The resulting power dissipation is proportional to the area of the B–H curve for the block material and the field excitation frequency. These losses can be very substantial or even exceed eddy current losses at sufficiently high frequencies.

C. Mechanical Heating

Small magnetizable particles suspended in a viscous solvent can physically spin in a time-varying magnetic field. The resulting mechanical motion may create significant frictional heating. We speculate that this may be a heating mechanism in some ferrofluids.

IV. Power Electronics

Two prototype power circuits were built to demonstrate the activation methods just described. Key considerations in the design of the prototypes were flexibility, power consumption, and portability. The resulting designs employ two different circuit topologies: the zero-voltage-switching (ZVS) full bridge shown schematically in Fig. 3 and the resonant class E converter shown in Fig. 5. Each circuit is discussed in the subsections that follow.

The function of the power circuit is to impress an ac waveform across an air-core solenoid (the induction coil) which surrounds the sample to be induction heated. The combination of the solenoid and test sample form a load that is most easily thought of as an air-core transformer with a shunted secondary winding. Schematically, this load is modeled as shown in Fig. 2. The resistance R_P represents the parasitic winding resistance of the solenoid. The resistance R_L accounts for the real power dissipation in the test sample. It is important to note that, in our experiments, poor coupling exists between the primary and secondary of the transformer because the sample occupies only a tiny fraction of the volume within the solenoid. This makes it reasonable to ignore the effects of the load resistance R_L and, thus, simplify the load model as shown. Also, any change in inductance that results from insertion or removal of the sample is small. Although the parameters L_H and R_P vary with frequency, they may be treated as constants under fixed-frequency operation.

A. ZVS Full Bridge

The first prototype, a full-bridge inverter, impresses a 240-kHz ac square wave across the load using four switches in an H-bridge configuration (see Fig. 3). The switches were implemented with IRFP450 MOSFET's. Gate drive isolation for the high-side switches was accomplished through pulse

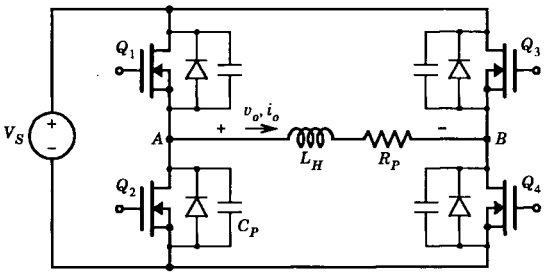

Fig. 3. Simplified ZVS full bridge schematic.

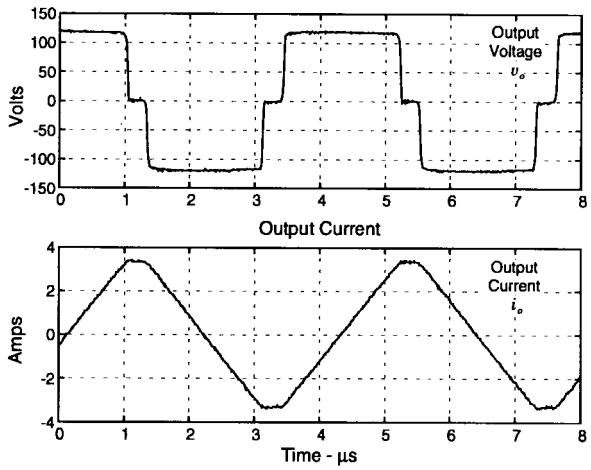

Fig. 4. ZVS full-bridge experimental waveforms at 240 kHz.

transformers. The MOSFET's Q_1–Q_4 are switched at a 100% duty-ratio using a phase-shifted pattern, as discussed in [14]. This technique allows the inductor current to ring with the parasitic capacitance C_P of the MOSFET's, which enables ZVS and significantly reduces switching losses. The primarily inductive load provided by the coil allows for ZVS under all heating conditions.

The bridge operates from a 120-V dc bus, which is stepped-up from a 24-V battery pack using a boost converter. As a result, the entire system is portable. The bus voltage is flexible, but limited by the 500-V breakdown voltage of the MOSFET's. The prototype outputs a $\pm$120-V square wave at 240 kHz. This results in a triangular ac current ($\approx\pm$4 A) through the load solenoid. Output waveforms, v_o and i_o, from the first prototype are pictured in Fig. 4. The inductance of the load solenoid L_H was 30.2 μH. The coil was constructed by winding 44 turns of multistrand litz wire on a 5.5-cm long plexiglass former. The system develops a peak H-field intensity of approximately 2500 A $\cdot$ T/m at the center of the solenoid.

The first prototype is well-suited for triggering gel samples seeded with lumped materials (method 1). Its most valuable asset is its ability to operate with ZVS over a wide range of load inductance. This allows the user to exchange, for instance, the 30.2-μH output solenoid with a 60.0-μH Helmholtz coil without adjusting the circuit parameters. Zero-voltage-switching is possible as long as the amplitude of the voltage ring V_{ring} at nodes A and B exceeds the bus voltage V_S as

TABLE I
LOSS BREAKDOWN FOR THE ZVS FULL BRIDGE

Source	Loss
Gate Drive & Logic	5.4 W
FET Conduction	4.5 W
Coil Conduction	5.5 W
Boost Converter	2.7 W
Total	18.1 W

shown by

$$V_{\text{ring}} = \left(I_{\text{pk}} \sqrt{\frac{L_H}{2C_P}} \right) > V_S. \tag{6}$$

Assuming a square-wave output and a purely inductive load we can express I_{pk} as

$$I_{\text{pk}} = \frac{V_S}{4L_H f_s} \tag{7}$$

where f_s is the switching frequency. It is now possible to define an upper limit for L_H under which ZVS can be sustained as follows:

$$L_H < \frac{1}{32C_P f_s^2}. \tag{8}$$

Substituting values for C_P and f_s of 720 pF and 240 kHz into (8), we find an upper limit on L_H of 754 μH.

Operating as in Fig. 4, the prototype consumes about 18.1 W, excluding power delivered to the load. A breakdown of the losses are given in Table I. The relative performance of the circuit for the induction-heating application can be judged by comparing the reactive power P_r flowing through the induction coil to the total real power dissipation in the circuit. A relationship between H-field intensity and reactive power is derived in the next subsection. The measured waveforms in Fig. 4 demonstrate a reactive power P_r of 253 VA. Therefore, we can define a figure of merit Q_{circuit} for this prototype as the ratio of reactive power to power loss as follows:

$$Q_{\text{circuit}} = \frac{253 \text{ V} \cdot \text{A}}{18.1 \text{ W}} = 14.0. \tag{9}$$

The full-bridge circuit meets all the design goals. The circuit is flexible, tolerant to load variations, portable, and consumes relatively little power. However, the circuit is not easily adapted for use at the higher frequencies (several megahertz) required to activate gels seeded with methods 2 and 3. As the switching speed is increased, it becomes apparent that the full-bridge topology has several disadvantages. First, the complex gate-drive circuitry of the full bridge quickly leads to considerable gate-drive losses, and tolerances must be tight in order to avoid catastrophic shoot-through. Second, high current and voltage derivatives during switching often excite unwanted resonances between device parasitic inductances and capacitances. Extreme care must be taken during circuit layout to minimize these unwanted resonances and the resulting increase in losses. Third, the bus voltage can quickly reach unreasonable levels (thousands of volts) when only a few amps are driven through a 30.2-μH coil at 2 or 3 MHz. A matching transformer is the obvious solution to this last problem, but the design of a low-loss, high-power, high-frequency transformer presents its own challenges. The most logical solution to this problem is, then, to employ a resonant converter topology.

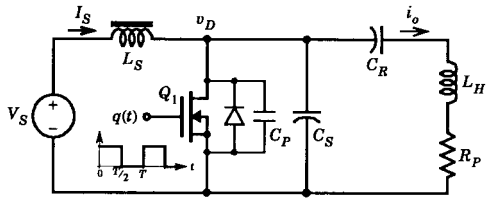

Fig. 5. Simplified class E schematic.

B. Resonant Class E Converter

The second prototype was built using a resonant class E topology developed by Sokal and Sokal in [15]. The class E converter is a current-fed, resonant, dc-to-ac converter that has been studied extensively [16]–[18]. A simplified schematic of the converter is shown in Fig. 5. A resonant capacitor C_R is placed in series with the output inductor L_H. A single switch, shunted by the capacitance C_S is used to gate the input current at a 50% duty cycle. The switching frequency f_s is fixed just above the resonant frequency, where the resonant frequency is defined as

$$f_r = \frac{1}{2\pi} \sqrt{\frac{1}{L_H C_R}}. \tag{10}$$

The parasitic resistance R_p is small in this case, so the Q of the series-resonant load is very high. This assures a current i_o through the load that is nearly a perfect sinusoid at the drive frequency. If the value of the shunt capacitor C_S is carefully selected, the drain-to-source voltage v_D of the MOSFET switch will ring, almost sinusoidally, from zero to its peak and then return toward a negative value. However, the MOSFET's antiparallel diode will begin to conduct as v_D goes negative, which clamps the voltage near zero. This sequence achieves ZVS over a limited range of load variation. In practice, the circuit is "tuned" by adjusting f_s and V_S until ZVS operation occurs. The switch must be sized to carry a peak current of $i_o + I_s$ and a peak voltage significantly above V_S. This results in a high switch stress, which is a disadvantage of the class E circuit.

The second prototype was designed to operate over a 1–3-MHz range. The higher frequency was necessary to test seeding methods 2 and 3. Switch Q_1 was realized using two IRFP450 MOSFET's in parallel for low on-state drain-to-source resistance and, thus, increased current capacity. The 500-V drain-to-source breakdown voltage of the IRFP450 provided a more than sufficient range for experimentation. Two new induction coils were wound. The first, coil A, is a 4.54-μH solenoid wound with 29 turns of 1700-strand, 48-AWG litz wire on a 5.85-cm long by 1.6-cm diameter former. The second, coil B, is a 12.89-μH solenoid wound with 28 turns of 1700-strand 48-AWG litz wire on a 5.72-cm long by 2.83-cm diameter former. The exceptionally high strand count litz wire is required to minimize ohmic power losses in the induction coil, which result from high-frequency skin effects

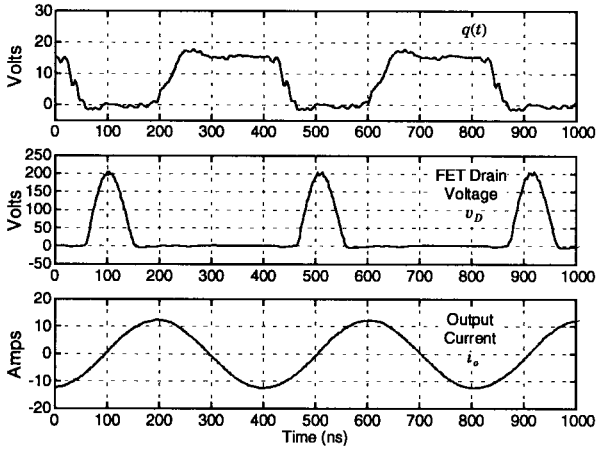

Fig. 6. Class E experimental waveforms at 2.5 MHz.

TABLE II
LOSS BREAKDOWN FOR THE CLASS E CIRCUIT

Source	Loss
Gate Drive & Logic	18.2 W
FET Conduction	22.2 W
Coil Conduction	89.8 W
Cooling Fan	5.0 W
Total	135.2 W

in the wire. The Q values of the two solenoids, measured at 2.5 MHz, are 117 and 170, respectively. The resonant capacitor C_R was selected according to (10) (720 pF for coil A and 300 pF for coil B). The capacitor C_S was eliminated, relying instead on the parasitic drain-to-source capacitance C_P of the paralleled MOSFET's (approximately 1440 pF).

Experimental waveforms are shown in Fig. 6. The figure shows the circuit operating with coil B and $f_s = 2.46$ MHz. The output current is sinusoidal at ± 12.5 A, yielding a peak H-field intensity of 5500 A $\cdot$ T/m. The input voltage V_S was set to 28 Vdc. The input current I_S was measured at 4.0 A. Under the operating conditions just described, the second prototype consumes 135.2 W, excluding power delivered to the load. A breakdown of the losses are given in Table II.

As with the ZVS full bridge, the ratio of the reactive power P_r across the coil and the total real power dissipation in the circuit serves as a performance indicator. Since the class E converter produces a sinusoidal load voltage and current, a relationship between the H-field intensity inside the induction coil and the reactive power across it can be analytically derived as follows. The reactive power across the coil is

$$P_r = I_{\rm rms}^2 X_l = I_{\rm pk}^2 \pi L f_s \tag{11}$$

where X_l is the impedance of the coil inductance and f_s is the switching frequency. The variables $I_{\rm rms}$ and $I_{\rm pk}$ represent the rms and peak values of the coil current, respectively. Now, substitute L in (11) with the inductance of a long solenoid,

$$L = \frac{\mu_o N^2 A}{l} \tag{12}$$

where μ_o is the permeability of free space, N is the number of turns, A is the cross-sectional area, and l is the length. Solving the result for $I_{\rm pk}$ and substituting into (1), we find the peak H-field intensity to be

$$H_{\rm pk} = k_d \sqrt{\frac{P_r}{\pi f_s \mu_o A l}} = k_d \sqrt{\frac{P_r}{\pi f_s \mu_o V_l}} \tag{13}$$

where V_l is the volume contained by the solenoid and

$$k_d = \frac{l/d}{\sqrt{1 + (l/d)^2}}. \tag{14}$$

The peak H-field intensity increases with the square-root of the reactive power P_r. Therefore, under the stated assumptions, the reactive power absorbed by the coil inductance is an indicator of the real power dissipation which could be induced in the target seed.

The waveforms in Fig. 6 demonstrate a reactive power P_r of 15.3 kVA. We can again define a figure of merit $Q_{\rm circuit}$ for this prototype as the ratio of reactive power to power loss

$$Q_{\rm circuit} = \frac{15.3\ {\rm kVA}}{135.2\ {\rm W}} = 113.2. \tag{15}$$

The performance of the class E circuit is clearly superior to that of the ZVS full bridge presented above. The theoretical limit for $Q_{\rm circuit}$ is the Q value of the induction coil itself. Despite the disadvantages of high switch stress and "tuning" difficulties, the class E circuit appears to be the best choice for this induction heating application.

V. RESULTS

Initial evaluations of the ZVS full-bridge and class E converters were conducted in the test stand with gels seeded by method 1. Both converters were adequate to trigger gels seeded with macroscopic pins with large dimensions as compared to the skin depth. For the smaller seed powders employed with method 2, the higher frequency (1–3 MHz) capability of the class E converter was essential to achieve adequate dissipation in the seed materials. High-frequency fields were also found to be essential to generate sufficient heating in the ferrofluids employed in method 3.

Fig. 7 shows the equilibrium phase transition curve of a NIPA gel seeded with method 2. Gels were seeded with Novamet nickel "leafing grade" flakes using the procedure described for method 2 in Section II. The curve in Fig. 7 shows the normalized gel diameter on the vertical axis versus peak current in induction coil A on the horizontal axis. A CCD video micrometer, illustrated in Fig. 1, was used during the course of the experiment to observe the gel diameter through a fractional gap in the solenoidal winding. A total of 18 diameter measurements were made. At each point, the gel was exposed to the magnetic field induced by the indicated coil current until the gel diameter equilibrated. The peak coil current can be related to magnetic field intensity using (1). The dashed line interpolating the points in the figure serves as a guide for the eye.

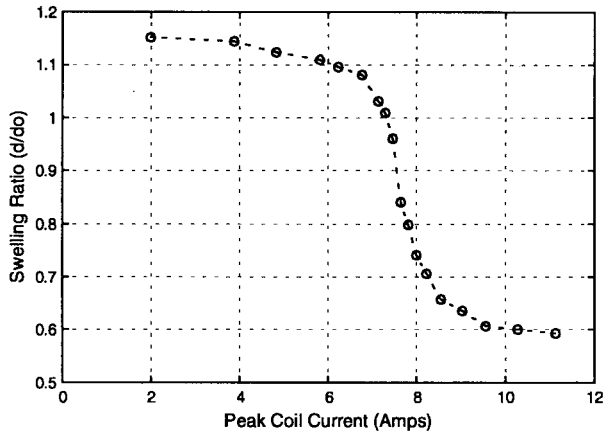

Fig. 7. Equilibrium gel diameter vs. current. The circulating water temperature is fixed at 30.0 °C.

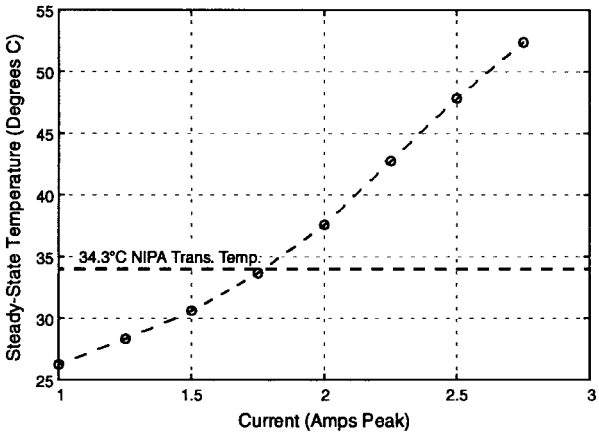

Fig. 9. Equilibrium ferrofluid temperature vs. current. The circulating water temperature is fixed at 22.0 °C.

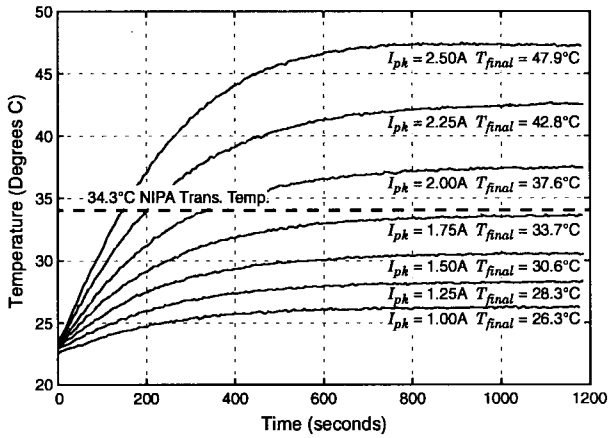

Fig. 8. Ferrofluid temperature versus time. The circulating water temperature is fixed at 22.0 °C.

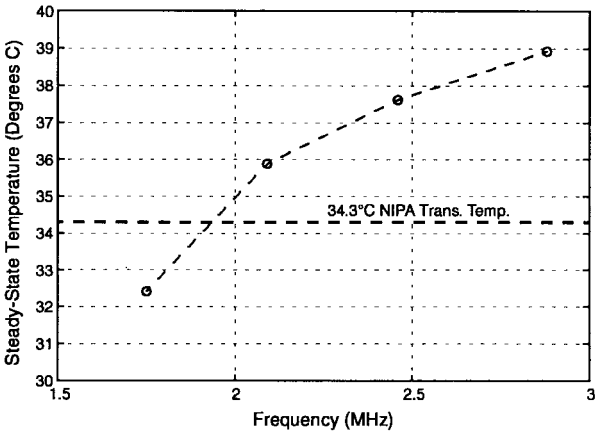

Fig. 10. Equilibrium ferrofluid temperature versus frequency. The circulating water temperature is fixed at 22.0 °C.

Tests to verify the efficacy of seeding method 3 were also conducted. We experimented with gels employing Ferrofluidics EMG 705[2] ferrofluid as a solvent. Qualitatively, we were able to observe magnetically activated phase transitions in these gels through before-and-after observation of the gel diameter. However, it was not possible to make real-time observations of the gel dimensions, due to the extreme opacity of the EMG 705 fluid. Instead, quantitative measurements of the ferrofluid temperature were made in the test stand using an Everest 4000.4GH[3] infrared pyrometer in place of the video microscopy system described above. The class E prototype with coil B, formed on a Liebig condenser, was used in the test stand, both to accommodate the larger ferrofluid sample sizes and also to provide an unobstructed axial view for the pyrometer. A test sample composed of 2 cc of ferrofluid in a glass vial was used for the experimental results shown in Figs. 8–10.

Fig. 8 shows the temperature rise in the ferrofluid sample versus time at seven different induction coil currents. Steady-state temperature values for the ferrofluid versus peak coil current are plotted in Fig. 9. The interpolating lines are again provided as guides for the eye. NIPA polymer gels undergo phase transition around 34.3 °C [4]. The dashed horizontal lines in Figs. 8 and 9 indicate the NIPA phase transition temperature for comparison with the dynamic and steady-state induction heating performance of the ferrofluid.

Finally, Fig. 10 shows the steady-state temperature of the ferrofluid sample at a fixed coil current of 2.0-A peak versus four different current/field frequencies. The horizontal dashed line again shows the NIPA phase transition point. It was necessary to retune the resonating elements (series capacitor C_R) at each desired operating frequency to maintain a proper operating point for the class E converter.

VI. Discussion

Magnetically activated phase transition polymer gels have a tremendous range of potential application. The three different seeding methods described in this paper provide the opportunity to optimize gel performance, chemical composition, and form factor for specific applications. We are considering the use of gels seeded with methods 1 and 2 for applications with *in vivo* drug delivery systems, actuators (synthetic muscles), and multipart industrial chemical delivery systems (where

[2] Ferrofluidics Corporation, 40 Simon Street, Nashua, NH 03061 USA.

[3] Everest Interscience Inc., 1625 West Ina Road, Suite 123, Tescon, AZ 85704 USA.

the gel is loaded with an appropriate chemical or medicinal solvent). In chemical delivery and actuator applications, magnetic activation, unlike many heating methods, can provide a swift, remotely activated phase transition. These qualities have also proven essential, for example, in developing practical servomechanical systems with polymer gels [19].

We are considering the application of gels seeded with method 3 for the creation of fluids that exhibit a variable viscosity in response to an applied magnetic field. For example, we have loaded ferrofluids with millimeter- to micrometer-diameter gel beads. When the beads are small, they occupy a small fraction of the solution volume, and the viscosity of the solution is essentially that of the surrounding ferrofluid. When the beads swell, they occupy a substantial part of the solution volume, and the overall solution exhibits a higher viscosity. With magnetic triggering, these fluids could be used to create remotely activated clutching mechanisms, vibration dampers, and molding systems.

This paper has presented and demonstrated the performance of practical power electronic drives for induction heating magnetically triggerable gels. These converters can be used with a variety of different gel systems and induction coil configurations to tailor the design of gel-based servomechanisms. By measuring slight changes in converter operation and coil parameters, it should be possible to actually estimate, in real time, the mechanical state of a magnetically responsive gel. Such an estimator could eventually be used to provide essential feedback information for closed-loop servomechanisms employing magnetically activated gels as actuators.

ACKNOWLEDGMENT

The authors gratefully acknowledge the valuable advice and support of Prof. T. Tanaka, Prof. M. Zahn, Prof. J. Kirtley, Prof. D, Sadoway, Prof. M. Kastner, Dr. X. Yu, and Dr. K. Raj. D. Evangelista and S. Shaw provided important assistance with the experiments presented. Essential materials were provided by Novamet Specialty Products Corporation and Ferrofluidics Corporation.

REFERENCES

[1] T. Tanaka, "Gels," *Scientific American*, vol. 244, no. 1, pp. 124–138, Jan. 1981.
[2] T. Tanaka, I. Nishio, S. Sun, S. Ueno-Nisho, "Collapse of gels in an electric field," *Science*, vol. 218, no. 29, pp. 467–469, Oct. 1982.
[3] A. Suzuki and T. Tanaka, "Phase Transition in Polymer Gels Induced by Visible Light," *Nature*, vol. 346, no. 6282, pp. 345–347, July 1990.
[4] S. Hirotsu, Y. Hirokawa, and T. Tanaka, "Volume-phase transitions of ionized N-isopropylacrylamide gels," *J. Chem. Phys.*, vol. 87, no. 2, pp. 1392–1395, July 1987.
[5] A. Mitwalli, S. Leeb, T. Tanaka, and U. Sinha, "Polymer gel actuators-status report," in *Proc. Universities Power Engineering Conf.*, 1994, pp. 871–874.
[6] H. A. Haus and J. R. Melcher, *Electromagnetic Fields and Energy*. Englewood Cliffs, NJ: Prentice-Hall, 1989.
[7] S. Haider, T. Cetas, J. Wait, and J. Chen, "Power absorption in ferromagnetic implants from radio frequency magnetic fields and the problem of optimization," *IEEE Trans. Microwave Theory Tech.*, vol. 39, pp 1817–1827, Nov. 1991.
[8] A. Mitwalli, S. Leeb, D. Jackson, D. Fusco, and T. Tanaka, "Phase transition in polymer gels induced by magnetic fields," in preparation.
[9] Raychem Corporation, "Induction heating of loaded materials," U.S. Patent 05 378 879, Jan. 1995.
[10] S. Ramo, J.R. Whinnery, and T. Van Duzer, *Fields and Waves in Communication Electronics*. New York: Wiley, 1984.
[11] R. Bozorth, *Ferromagnetism*. Piscataway, NJ: IEEE Press, 1993.
[12] M. Zahn, "Power dissipation and magnetic forces on MAGLEV rebars," *IEEE Trans. Magn.*, to be published.
[13] P. D. Agarwal, "Eddy-current losses in solid and laminated iron," *AIEE Trans. Commun. Electron.*, vol. 78, pt. I, pp. 169–179, May 1959.
[14] L. Mweene, C. Wright, and M. Schlecht, "A 1 kW, 500 kHz front-end converter for a distributed power supply system," in *Proc. IEEE-APEC*, 1989, pp. 423–432.
[15] N. Sokal and A. Sokal, "Class E - A new class of high efficiency tuned single-ended switching power amplifier," *IEEE J. Solid-State Circuits*, vol. SC-13, pp. 168–176, Mar. 1975.
[16] D. Collins, S. Hinchliffe, and L. Hobson, "Computer control of a class-E amplifier," *Int. J. Electron.*, vol. 64, no. 3, pp. 493–506, 1988.
[17] S. Hinchliffe and L. Hobson, "High efficiency DC-AC converters suitable for high frequency induction process heating," in *Conf. Rec. PESC'88*, 1988, pp. 1228–1235.
[18] F. H. Raab, "Idealized operation of the class E tuned power amplifier," *IEEE Trans. Circuits Syst.*, vol. CAS-24, pp. 725–735, Dec. 1977.
[19] A. Mitwalli, Ph.D. dissertation, M.I.T., Cambridge, MA, expected 1997.

Deron K. Jackson received the B.S. degree in electrical engineering from the University of California at Davis, in 1991 and the M.S. degree in electrical engineering from Massachusetts Institute of Technology, Cambridge, in 1994. He is currently working toward the Ph.D. degree at the Massachusetts Institute of Technology Laboratory for Electromagnetic and Electronic Systems.

His research interests are in the area of power electronics and control.

Steven B. Leeb (S'89–M'91) received the B.S., M.S., E.E., and Ph.D. degrees from the Massachusetts Institute of Technology, Cambridge, in 1987, 1989, 1990, and 1993, respectively.

Since 1993, he has been a faculty member with the Department of Electrical Engineering and Computer Science, Massachusetts Institute of Technology. He currently serves as the Carl Richard Soderberg Assistant Professor of Power Engineering in the Laboratory for Electromagnetic and Electronic Systems. He is concerned with the design, analysis, development, and maintenance processes for all kinds of machinery with electrical actuators, sensors, or power electronic drives.

Dr. Leeb is a member of the IEEE Power Electronics, Control Systems, Power Engineering, and Signal Processing Societies. He is a fellow of M.I.T.'s Leader's for Manufacturing Program and a member of Tau Beta Pi and Eta Kappa Nu.

Ahmed H. Mitwalli received the B.S. and M.S. degrees in electrical engineering from the Massachusetts Institute of Technology, Cambridge, in 1991 and 1993, respectively. He is currently working toward the Ph.D. degree at the Massachusetts Institute of Technology Laboratory for Electromagnetic and Electronic Systems.

His research is in the development of novel actuator technologies (specifically polymer gel actuators), with emphasis on system identification and control.

Mr. Mitwalli is a member of Tau Beta Pi, Eta Kappu Nu, and Sigma Xi.

Paolo Narvaez received the B.S. degree from Massachusetts Institute of Technology, Cambridge, in 1996. He is currently is a graduate student in the Department of Electrical Engineering and Computer Science, Massachusetts Institute of Technology.

Dahlene Fusco is an undergraduate student in physics and philosophy at Wellesley College, Wellesley, MA.

Elmer C. Lupton, Jr. received degrees in chemistry from Massachusetts Institute of Technology, Cambridge, and Yale University, New Haven, CT.

He has held technical and managerial positions with the U.S. Air Force, Allied Chemical Corporation, Composite Container Company, Maryland Cup Corporation, Panelgraphic Corporation, ICI Incorporated, and CHEMFAB Corporation. He is currently Vice President and Chief Technical Officer of Gel Sciences Incorporated, Bedford, MA, and is directing the development and application of responsive gels for a number of industry areas including power and energy distribution, petroleum production, medical/pharmaceutical, cosmetics, automotive, and paints and coatings. He is the author of several technical publications and patents.